The 10th JFPS International Symposium on Fluid Power FUKUOKA 2017 Oct. 24-27, 2017 The Japan Fluid Power System Society

JET CAVITATION EROSION OF HOLLOW CYLINDERS (An Experimental Investigation into the Effects of Chamfers and Tapers)

Toshiharu KAZAMA*, Kento KUMAGAI**, Ikuya SAKAMI***, and Yukihito NARITA***

*College of Design and Manufacturing Technology, Muroran Institute of Technology
27-1, Mizumoto-cho, Muroran, Hokkaido, 050-8585, Japan
(E-mail: kazama@mmm.muroran-it.ac.jp)
** Hitachi Construction Machinery Co., Ltd. (650, Kandatsu, Tsuchiura, Ibaraki 300-0013, Japan).
*** Muroran Institute of Technology (27-1, Mizumoto-cho, Muroran, Hokkaido, 050-8585, Japan).

Abstract. Erosion at the inner walls of hollow cylinders, in which cavitating jets flowed, was investigated experimentally using the jet cavitation erosion tester. Aluminum specimens with the representative size of 20 mm length, 20 mm outer diameter, and 5 mm inner diameter were prepared. The chamfered specimens had chamfers of 0.5, 1, 3, and 5 mm; the tapered specimens had tapers of 2.9°, 5.7°, 11.5°, and 17.2°. The test fluid was hydraulic oil with a viscosity grade of 32. The specimens were halved and observed after the experiment. In parallel, the cavitating jets were observed using a high-speed video camera. The inner walls of the chamfered specimens were partially eroded at a slightly shorter distance from the chamfered edge of the downstream side, regardless of the chamfer magnitude. The erosion of divergent tapered specimens was not confirmed under the conditions.

Keywords: Cavitation, Erosion, Jet, Hydraulics, Geometry

INTRODUCTION

Cavitation erosion [1, 2] in fluid machinery is predominantly caused by the collision of submerged cavitating jets [3] and collapsing bubbles [4]. Using a prototype based on the Lichtarowicz apparatus [5], many researchers have studied the erosion [6–10] caused by cavitating jets [11, 12]. However, in these studies, water was used as the test liquid [13] and the jets were impinged vertically, and occasionally obliquely [14], onto the specimen surfaces. There are few reports on erosion at the walls of the flow paths by cavitating jets with oils.

Erosion is also a serious problem in hydraulic equipment [15, 16], such as hydraulic valves, positive displacement pumps, and motors. In certain situations, erosion occurs in the channels and passages in which the jets flow, especially in pressure, flow, and directional control valves, where the jets do not exactly impinge directly onto the surfaces [17] of the inner walls. However, very few experiments have been performed to study the erosion at the walls along the flow paths by using cavitating oil jets.

In this study, we used hollow cylindrical specimens with chamfers and tapers and examined the effects of the geometry and flow on the location and magnitude of erosion. The eroded parts of the specimens were observed, and the effects of experimental conditions on cavitation erosion were investigated. In addition, we observed the cavitating jets using a high-speed video camera and compared the processed images with the eroded specimens.

TEST APPARATUS AND CONDITIONS

Test Apparatus

Figure 1 depicts the chamber, which is the main part of the test apparatus. The setup process, experimental conditions, and test procedures are discussed briefly here because the method used in this experiment is almost identical to that prescribed by the ASTM standards [18] and previously published papers [19, 20].

The hydraulic circuit consisted of the chamber, hydraulic power unit, hydraulic auxiliaries, and pressure and temperature sensors. The power unit had a positive displacement pump (maximum operating pressure of 40 MPa and discharge of 2.3×10^{-4} m^3/s), electric motor, and reservoir. The accessories included valves, cooler, filter (nominal pore size of 3 μm), and hoses. The sensors included pressure gages and a thermometer.

The chamber was made of stainless steel with two transparent windows on the sides. The inner diameter was 170 mm. The chamber included a long-orifice nozzle, holder to fix the nozzle, specimens (hollow cylinders), three struts and a mount to support the specimen, and spacers to adjust the location of the specimen. The nozzle had the flow path of 1 mm in diameter and 4 mm in length, and the flow path of the holder was 3 mm in diameter and 3 mm in length.

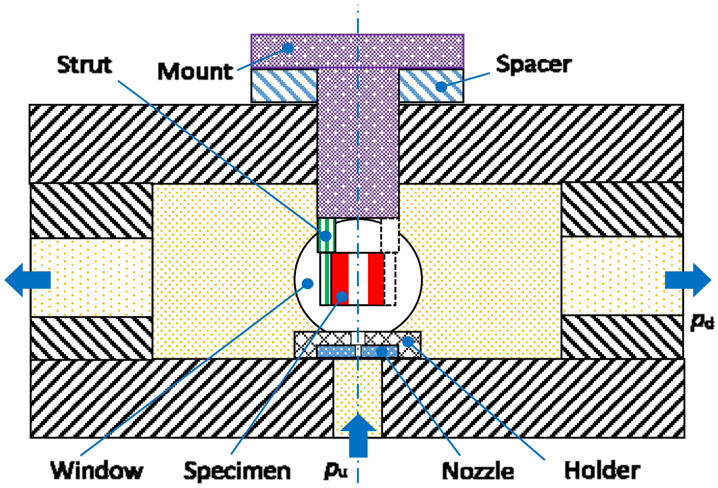

FIGURE 1. Test chamber.

Test Conditions

The hollow cylindrical specimens [21] were prepared from an aluminum alloy (Japan Industrial Standards, JIS A5056). The outer diameter and length of the specimens were 20 mm and 20 mm, respectively. In this experiment, two types of specimens were prepared; chamfered and tapered. For chamfered specimens, one end surface was chamfered at c = 0.5, 1, 3, or 5 mm with a typical angle of 45°, while the other end was light-chamfered. For tapered specimens, the tapers were set at 2.9°, 5.7°, 11.5°, and 17.2°, corresponding to the diameters of one end of the specimens to be 6, 7, 9, and, 11 mm and the other end to be 5 mm in all cases (designated as $\phi5$–$\phi6$, $\phi5$–$\phi7$, $\phi5$–$\phi9$, and $\phi5$–$\phi11$ for divergent specimens, and $\phi6$–$\phi5$, $\phi7$–$\phi5$, $\phi9$–$\phi5$, and $\phi11$–$\phi5$ for convergent specimens, respectively). By using these specimens, partial and whole, as well as divergent and convergent, flow paths were formed. The specimens were supported by three struts on the mount.
Because of the difficulties of machine processing, the hollows of the tapered specimens were manufactured by wire-cut electrical discharge machining, while the hollows of the chamfered specimens were bored by drilling. In addition, the eroded mass loss was infinitesimal, e.g., < 1 mg, up to t = 8 h under these experimental conditions. Thus, discussion of the aspects and the location of erosion can be meaningful, while a precise comparison of the eroded mass loss of specimens between the chamfered and tapered specimens may not be possible.
The stand-off distance L was defined as the distance between the edge-face of the nozzle outlet and the upstream-side end surface of the cylindrical specimens; the value of L was determined using annular spacers. The distance L was set to 15 mm, which was the condition for maximum erosion of a standard specimen without chamfer and taper. The test liquid used was a mineral-oil-type hydraulic fluid of ISO viscosity grade VG 32 (kinematic viscosities of 32.6 mm^2/s at 40 °C and 5.49 mm^2/s at 100 °C). The oil temperature was maintained at 40 °C ± 1 °C using an inline oil cooler. The test oil was recirculated and the air content was not controlled [22].
The cavitation number σ is defined as the ratio of the downstream absolute pressure p_d and the upstream pressure p_u. In the experiment, σ was set at 0.02 and p_u was maintained at 10.1 MPa
At the beginning of each test, the specimen was set, the chamber was filled with the test oil, and the remaining air and bubbles were carefully removed from the chamber. The submerged jet was cavitated through the nozzle and discharged into the chamber. The upstream and downstream pressures and the oil temperature were monitored continuously and controlled manually to maintain the prescribed experimental conditions during the test.
In parallel, transparent acryl-resin specimens were prepared and the cavitating jets in and around the specimens were preliminarily observed using a high-speed video camera (shortest exposure time 1 μs, full frame rate: 4000 fps, maximum frame rate: 800000 fps).

RESULTS AND DISCUSSION

Chamfered Specimens

Figure 2 shows cross-sectional photographs of the specimens with chamfers c = 0.5, 1, 3, and 5 mm. The specimens were cut using a precision machine tool after the completion of the experiments (accumulated exposure time t = 8 h). The conditions were as follows: inner diameter D_i = 5 mm, cavitation number σ = 0.02, and stand-off distance L = 15 mm. The direction of the flow was right to left in these photographs, and the chamfered end surfaces of the specimens were placed at the downstream side. Erosion is visible in all specimens. The eroded region was closed to the edge; but rather a slight distance from the end surface of the downstream side. As the chamfer became larger, the location moved to the upstream side. However, the distance from the outlet edge of the flow path, i.e., the circumferential line at intersection of the hollow path and the chamfer part, to the eroded region was nearly unchanged (approximately 1–2 mm). As a result, a chamfer at the downstream side did not impact the degree of erosion, and thus hardly contributed to reducing erosion.
Figure 3 shows photographs of the chamfered specimens where the direction of the flow was left to right- the chamfered end surfaces were placed at the upstream side. A similar degree of erosion was observed at the same location in all specimens. Therefore, a chamfer at the upstream side also did not influence the erosion.

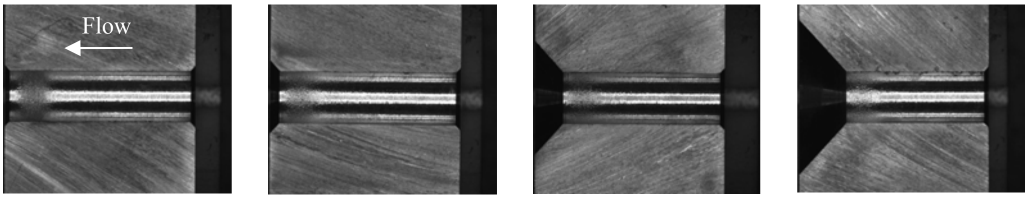

c = 0.5 mm c = 1 mm c = 3 mm c = 5 mm

FIGURE 2. Photographs of specimens chamfered at the downstream side, halved after experiment (D_i = 5 mm, σ = 0.02, L = 15 mm, t = 8 h).

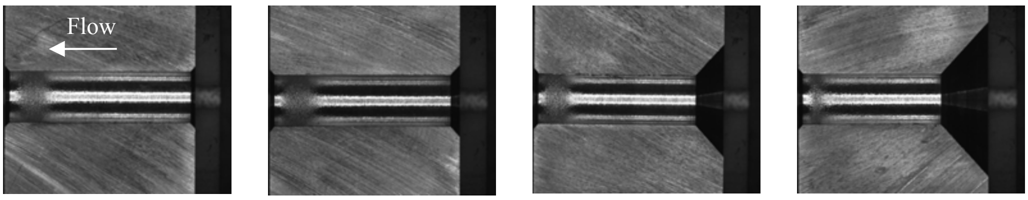

c = 0.5 mm c = 1 mm c = 3 mm c = 5 mm

FIGURE 3. Photographs of specimens chamfered at the upstream side, halved after experiment (D_i = 5 mm, σ = 0.02, L = 15 mm, t = 8 h).

Tapered Specimens

Figures 4 and 5 show the tapered specimens cut into halves after the experiment (t = 8 h). The flow direction is right to left. Photographs in Fig. 4 are the results of the divergent path and those in Fig. 5 are the results of the convergent path. Although it is difficult to convey with these pictures, the erosion pits were visible in the convergent path specimens, but not in the divergent specimens.
The end surfaces of the specimens were also carefully examined. However, erosion could not find almost all specimens. It should be noted here that minor defects (burrs) were observed at the outlet edge of the largely converged specimens, e.g., D_i = ϕ11–ϕ5.

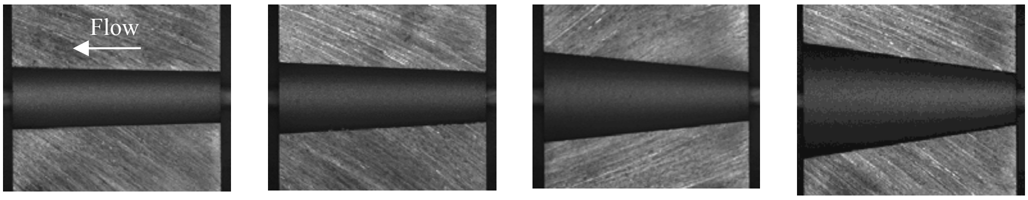

D_i = ϕ5–ϕ6 D_i = ϕ5–ϕ7 D_i = ϕ5–ϕ9 D_i = ϕ5–ϕ11

FIGURE 4. Photographs of divergent tapered specimens, halved after experiment (σ = 0.02, L = 15 mm, t = 8 h).

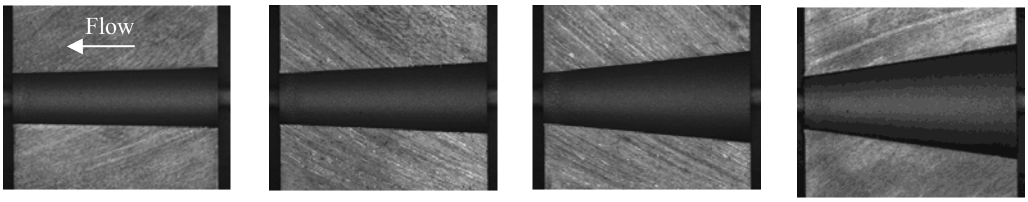

D_i = ϕ6–ϕ5 D_i = ϕ7–ϕ5 D_i = ϕ9–ϕ5 D_i = ϕ11–ϕ5

FIGURE 5. Photographs of convergent tapered specimens, halved after experiment (σ = 0.02, L = 15 mm, t = 8 h).

Figures 6 and 7 are photographs of the end surfaces of the specimens after the experiment, corresponding to Figs. 4 and 5, respectively. The upper and lower pictures are the end surfaces at the upstream and downstream sides, respectively. Erosion pits and damages were not visible in any of the specimens as shown in these photographs, except for specific specimens, e.g., D_i = ϕ11–ϕ5.

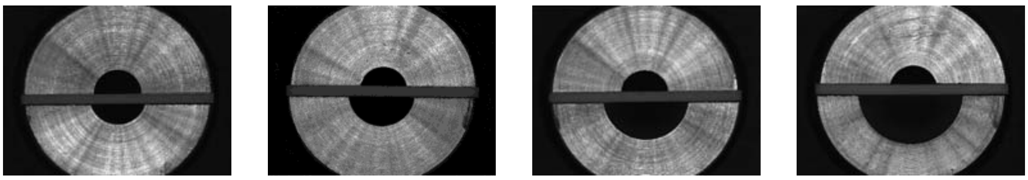

D_i = ϕ5–ϕ6 D_i = ϕ5–ϕ7 D_i = ϕ5–ϕ9 D_i = ϕ5–ϕ11

FIGURE 6. Photographs of end surfaces of divergent tapered specimens (upper: upstream side, lower: downstream site: D_i = 5 mm, σ = 0.02, L = 15 mm, t = 8 h).

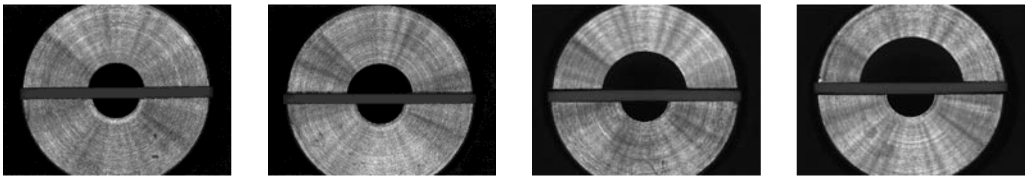

$D_i = \phi6–\phi5$ $D_i = \phi7–\phi5$ $D_i = \phi9–\phi5$ $D_i = \phi11–\phi5$

FIGURE 7. Photographs of the end surfaces of convergent tapered specimens (upper: upstream side, lower: downstream site: D_i = 5 mm, σ = 0.02, L = 15 mm, t = 8 h).

Figure 8 shows magnified photographs close to the downstream end surface of the inner surfaces of the flow paths of the divergence (a: ϕ5-ϕ11) and convergence specimens (a: ϕ11-ϕ5), where the jets flowed from right to left. Corresponding to Fig. 8, Fig. 9 displays the surface profiles close to the downstream end surface of the inner surfaces of the flow paths of the tapered specimens. The surface of the convergent specimen was eroded at 1–2 mm from the downstream edge, whereas the divergent specimen exhibited some roughness and a smooth surface.

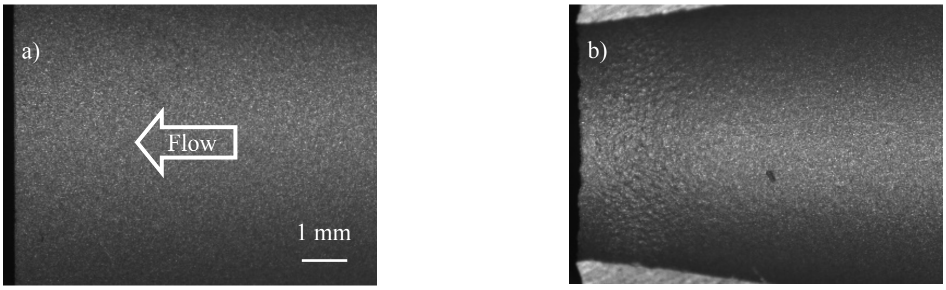

FIGURE 8. Eroded region of inner surfaces of halved specimens (L = 15 mm, t = 8 h, σ = 0.02; a: ϕ5-ϕ11, b: ϕ11-ϕ5).

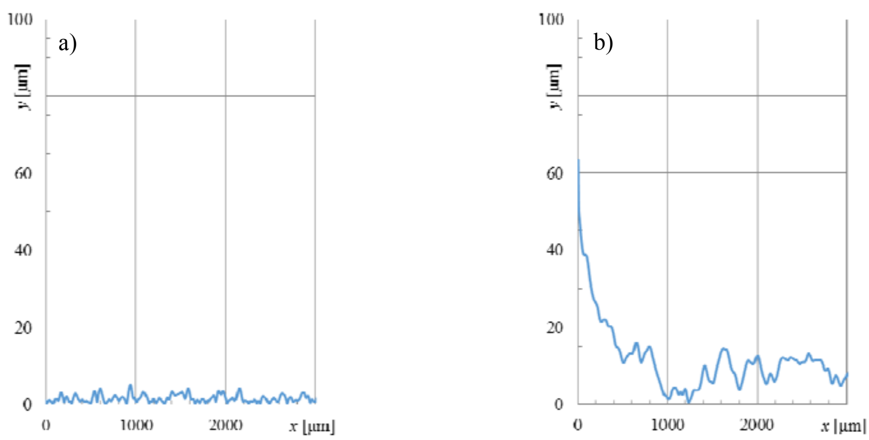

FIGURE 9. Surface profiles of halved specimens (L = 15 mm, t = 8 h, σ = 0.02; a: ϕ5-ϕ11, b: ϕ11-ϕ5).

Visualization of Cavitating Jet: Chamfered Specimens

Figures 10 and 11 show processed pictures of the cavitating jets using clear specimens chamfered at the downstream (Fig. 10) and the upstream sides (Fig. 11). The cylindrical specimens were made of acryl-resin and fabricated with chamfers of c = 1, 3, and 5 mm. The jets flowed from right to left in these pictures. The jets were recorded using a high-speed video camera under transmitted light, shutter speed 1/40000 s, and frame rate 32000 fps. The cavitating jets had an unsteady flow, so they were examined by time-integrated flow. Ten pictures were extracted from the video, and the processed pictures were made by superimposing these pictures. The clusters and clouds of cavitation bubbles and the bar of the two overlapped struts at the bottom are dark in the pictures because of the backlight.
Figures 10 and 11 show that the flows at the inlets and outlets of the hollow specimens with chamfers at the upstream and downstream sides were almost similar and the flows in the straight run of the circular tube paths were virtually the same. The effects of chamfers on the flows were not markedly recognized at this stage.

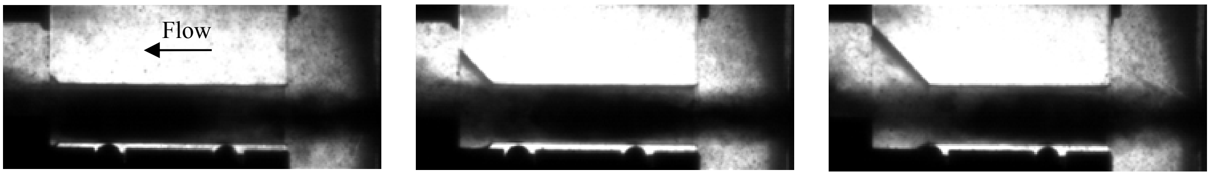

c = 1 mm c = 3 mm c = 5 mm

FIGURE 10. Processed pictures of cavitating jets using clear specimens chamfered at the downstream side.

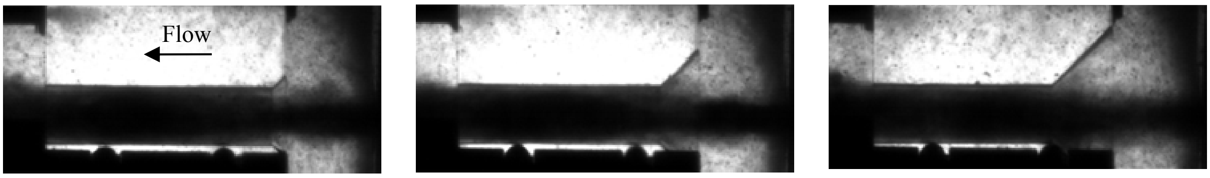

c = 1 mm c = 3 mm c = 5 mm

FIGURE 11. Processed pictures of cavitating jets using clear specimens chamfered at the upstream side.

CONCLUSIONS

This study examined the erosion of hollow cylinders by a cavitating jet. The effects of chamfers and tapers on the magnitude and location were examined experimentally to assess the erosion of oil-hydraulic valves. The salient conclusions are as follows:

i) For chamfered specimens, the inner walls were partially eroded at a slightly shorter distance from the chamfered edge of the downstream side. The aspect of erosion was not influenced by the chamfer magnitude.

ii) For tapered specimens, the inner walls of the straight and convergent tapered specimens were partially eroded close to the downstream surface end. In contrast, the divergent tapered specimens were not eroded under these experimental conditions.

ACKNOWLEDGMENTS

The authors would like to thank Mr. T. Noda of the Muroran Institute of Technology for his assistance.

APPENDIX

Nomenclature

c	Chamfer [mm]
D_i	Specimen inner diameter [mm]
L	Stand-off distance [mm]
p_d	Downstream absolute pressure [MPa]
p_u	Upstream absolute pressure [MPa]
t	Exposure time [h]
σ	Cavitation number = p_d / p_u

REFERENCES

1. KNAPP, R.T., DAILY, J.W., HAMMITT, F.G., Cavitation, 1970, McGraw Hill.
2. KATO, H., Cavitation, 1999, Maki-Shoten, (in Japanese).
3. WATANABE, R., YANAGISAWA, K., YAMAGATA, T., FUJISAWA, N., Simultaneous Shadowgraph Imaging and Acceleration Pulse Measurement of Cavitating Jet, Wear, Vol. 358–359, 2016, pp.72–79.
4. TOMITA, Y., SHIMA, A., Mechanisms of Impulsive Pressure Generation and Damage Pit Formation by Bubble Collapse, Journal of Fluid Mechanics, Vol. 169, 1986, pp.535–564.
5. LICHTAROWICZ, A., Use of a Simple Cavitating Nozzle for Cavitation Erosion Testing and Cutting, Nature, Physical Science, Vol. 239, No. 91, 1972, pp.63–64.
6. KLEINBREUER, W., Kavitationserosion in Hydraulischen Systemen, Industrie-Anzeiger, Vol. 99, No. 34, 1977, pp.609–613.
7. YAMAGUCHI, A., SHIMIZU, S., Erosion due to Impingement of Cavitating Jet, Journal of Fluids Engineering, Transactions of American Society of Mechanical Engineers, Vol. 109, No. 4, 1987, pp.442–447.
8. MOMMA, T. and LICHTAROWICZ, A., Study of Pressures and Erosion Produced by Collapsing Cavitation, Wear, Vol. 186–187, No. 2, 1995, pp.425–436.
9. SOYAMA, H., Effect of Nozzle Geometry on a Standard Cavitation Erosion Test Using a Cavitating Jet, Wear, Vol. 297, No. 1–2, 2013, pp.895–902.
10. HATTORI, S., GOTO, Y., FUKUYAMA, T., Influence of Temperature on Erosion by a Cavitating Liquid Jet, Wear, Vol. 260, Iss. 11–12, 2006, pp. 1217–1223.
11. PENG G., SHIMIZU S., Progress in Numerical Simulation of Cavitating Water Jets, Journal of Hydrodynamics, Ser. B, Vol. 25, Iss. 4, 2013, pp. 502–509.
12. KUMAGAI, K., RYU, S., KAZAMA, T.: Evaluation of Submerged Jet Cavitation Erosion with CFD, Proc. Japan Fluid Power System Society, Okinawa 2011, 1B1-3, pp. 116–121.
13. STELLER, J., International Cavitation Erosion Test and Quantitative Assessment of Material Resistance to Cavitation, Wear, Vol. 233–235, 1999, pp.51–64.
14. SUGIMOTO, Y., JIBIKI, Y., SATO, K., Behavior and Erosion of Cavitating Jet Impinging on Oblique Surface, Japanese Journal of Multiphase Flow, Vol. 24, No. 5, 2010, pp.697–702 (in Japanese).
15. BISHOP, R. J., Jr., TOTTEN, G. E., Effect of Pump Inlet Conditions on. Hydraulic Pump Cavitation: A Review, Hydraulic Failure Analysis: Fluids, Components, and. System Effects, ASTM STP1339, 2001, pp.318–332.
16. GOTO, H., SAKAMA, S., SUZUKI, R., Y. TANAKA, Y., Reduction of Cavitation Damage by Elimination of Bubbles in Oil Reservoir, Proc. The 12th International Symposium on Fluid Control, Measurement and Visualization, 2013, OS1-02-4.
17. PETKOVSEK, M., DULAR, M., Simultaneous Observation of Cavitation Structures and Cavitation Erosion, Wear, Vol. 300, Iss. 1–2, 2013, pp. 55–64.
18. ASTM, Standard Test Method for Erosion of Solid Materials by a Cavitating Liquid Jet, Annual Book of ASTM Standards, G134.95, 1995, pp.529–540.
19. KAZAMA, T., KUMAGAI, K., OSAFUNE, Y., NARITA, Y., RYU, S., Erosion of Grooved Surfaces by Cavitating Jet with Hydraulic Oil, Journal of Flow Control, Measurement & Visualization, Vol. 3, 2015, pp.41–50.
20. KAZAMA, T., MIURA, Y., Reduction in Submerged Jet Cavitation Erosion (Flow Control by Geometry Close to Nozzle Outlets and Impinged Surfaces), Transactions of Japan Fluid Power System Society, Vol. 38, No. 6, 2007, pp.77–82 (in Japanese).
21. KAZAMA, T., KOHIRUIMAKI, Y., KUMAGAI, K., Experiment on Erosion of Hollow Cylinders by Cavitating Jet of Hydraulic Oil, Mechanical Engineering Letters, Vol. 2, 2016, pp.16-00442.
22. SAKAMA, S., SUZUKI, R., TANAKA, Y., A Study on Design and Estimation of Bubble Eliminator (1st Report: Selection of Diameter of Vent Port)," Transactions of Japan Fluid Power System Society, Vol. 44, No. 2, 2013, pp. 43–48 (in Japanese).